Computer Vision and Image Understanding xxx (2009) xxx–xxx

Contents lists available at ScienceDirect

Computer Vision and Image Understanding

journal homepage: www.elsevier.com/locate/cviu

Laser range scanner based on self-calibration techniques using coplanarities and metric constraints

Ryo Furukawa [a,*], Hiroshi Kawasaki [b]

[a] Hiroshima City University, 3-4-1 Ozuka-higashi, Asaminami-ku, Hiroshima 731-3194, Japan
[b] Saitama University, 255 Shimo-ohkubo, Sakura-ku, Saitama 338-8570, Japan

ARTICLE INFO

Article history:
Received 1 May 2008
Accepted 15 May 2009
Available online xxxx

Keywords:
3D scanning
Light sectioning method
Self-calibration
Handheld laser scanner
Coplanarity
Shape reconstruction

ABSTRACT

In this paper, we propose a novel method to achieve both dense 3D reconstruction of the scene and estimation of the camera intrinsic parameters by using coplanarities and other constraints (e.g., orthogonalities or parallelisms) derived from relations between planes in the scene and reflected curves of line lasers captured by a single camera. In our study, we categorize coplanarities in the scene into two types: implicit coplanarities, which can be observed as reflected curves of line lasers, and explicit coplanarities, which are, for example, observed as walls of a building. By using both types of coplanarities, we can construct simultaneous equations and can solve them up to four degrees of freedom. To upgrade the solution to the Euclidean space and estimate the camera intrinsic parameters, we can use metric constraints such as orthogonalities of the planes. Such metric constraints are given by, for example, observing the corners of rectangular boxes in the scene, or using special laser projecting device composed of two line lasers whose laser planes are configured to be perpendicular.

1. Introduction

Line lasers are frequently used for active 3D scanning systems. In most of the systems, laser planes are calibrated first, and the points lit by the lasers are reconstructed by triangulation [1,2]. In these systems, known-shaped objects, or calibration markers are required to calibrate the laser planes.

Geometrically, a line laser can be considered as a device for extracting a set of points that exist on the same plane (coplanar points). Although coplanarity has been researched in single view reconstruction methods, this property of line lasers has not been fully utilized for active vision systems. By utilizing coplanarities extracted by line lasers, an active measurement system without need for explicit calibration of laser planes (planes formed by line lasers) can be realized.

In this study, we propose a method for estimating dense 3D shapes and the camera parameters by using information such as coplanarities that are extracted from curves on the scenes lit by line lasers (we call this type of coplanarity as *implicit coplanarity*), or from planes in the scenes (we call this type of coplanarity as *explicit coplanarity*). Fig. 1(left) shows an example of the system used to observe implicit and explicit coplanarities, where the target scene is captured by a fixed camera while the scene is lit by a line laser. By using this system, a large number of coplanarities can be also observed as curves that are reflection of the laser on the scene by capturing a sequence of images while moving the laser projector. By accumulating the curves of multiple images, a number of intersection points are extracted as shown in Fig. 1(right). In this paper, methods for reconstruction of 3D positions of the curves using the intersection points are presented.

Although coplanarities play an important role for shape reconstruction, they cannot be used for estimating the camera intrinsic parameters or for Euclidean reconstruction. For these purposes, we need other types of constraints (*e.g.*, orthogonalities or parallelisms). We call this kind of constraints *metric constraints.* Metric constraints can be extracted from relationships between real planes in the scene or laser planes. For example, we can obtain orthogonalities by using a laser projector composed of two line lasers with laser planes forming a right angle.

Reconstruction in the proposed method is realized by solving the simultaneous equations constructed from both the coplanarities and the metric constraints. As described later, coplanarity constraints can be described by linear equations, and metric constraints can be described by either linear or non-linear equations. The linear equations from coplanarity constraints can be solved only up to 4-DOF indeterminacies that are represented by projective transformation. Therefore, our method first solves linear simultaneous equations achieving *projective* reconstruction, and upgrades the solution to the Euclidean space. Depending on the representation of metric constraints that are either linear or

* Corresponding author. Fax: +81 82 830 1686.
E-mail addresses: ryo-f@cs.hiroshima-cu.ac.jp (R. Furukawa), kawasaki@cgv.ics.saitama-u.ac.jp (H. Kawasaki).

1077-3142/$ - see front matter © 2009 Elsevier Inc. All rights reserved.
doi:10.1016/j.cviu.2009.05.006

non-linear, two methods are presented in this paper. The method that uses linear representation can be applicable even if all the intrinsic parameters are unknown, as long as there are sufficient number of (at least nine) dependent constraints of orthogonalities. The linear method does not need an initial solution that is usually required for the non-linear method. However, if some or all of the intrinsic parameters are known, the method using non-linear representation is more stable and accurate.

Since we treat implicit and explicit coplanarities equally, our method is applicable even when there are no implicit coplanarities. In this case, a scene is reconstructed only from a single image *i.e.*, single view reconstruction). An advantage of our method compared to previous single view reconstruction methods is that our method is applicable for a scene that has enough geometrical constraints, but does not have special features for self-calibration, such as rectangular boxes or vanishing points with known angles between them.

2. Related works

There are many active stereo range finders using structured light including commercial products [1,2], and 3D reconstruction techniques are summarized in some survey papers [3,4]. With those systems, the laser plane is fixed, or controlled by precision mechanical devices. For these systems, laser plane calibration is required and precise calibration should be applied previously [5–7]. Some researches were focused on self-calibration of cameras and projecting devices for active stereo range finders [8–10].

In the case of a handheld laser 3D scanner, which is recently attracting wide attention because of its maneuverability and simplicity, the relationship between the laser plane and the camera position varies every time and must be calibrated online. For example, Chu et al. have proposed an explicit calibration using a cubic frame surrounding the target object [11]. Bouguet and Perona proposed a 3D scanner using "shadow planes" cast by a straight-edged object that is calibrated by a reference plane [12]. Fisher et al. also used shadows of a straight-edged object, whose position and orientation were estimated (*i.e.*, calibrated) from observed patterns printed on the surface of the object [13]. Furukawa and Kawasaki placed LED markers on the sensor itself and captured the markers with a single camera to estimate the laser plane [14]. The above-mentioned methods solved the online laser plane calibration problems, however, they still require an object or markers for calibration. Recently, Furukawa et al. proposed a method which does not require an object in order to calibrate the laser plane, but self-calibrates it [15]. However, the method requires precise initial parameters, special capturing device and strict conditions for scanning.

There are some handheld 3D scanners in which the laser plane projector and a camera are at a fixed position to each other [16,17]. Such devices require laser plane calibration only once, and thus, the special laser plane calibration method is not usually necessary.

With regard to single view reconstructions, most techniques including ours perform the self-calibration of the camera parameters for 3D reconstruction. For the purpose, some studies use multiple vanishing points [18–22]. In those studies, angles between the directions corresponding to the vanishing points should be known for the self-calibration. There are other techniques that directly use the rectangular boxes or the parallelepipeds [23,24]. In contrast to these methods, our method can use any type of metric constraints as long as they can be expressed as equations of points, planes or lines: thus, in some cases, our method can solve problems that cannot be solved by the previous methods.

Some researchers have proposed methods for 3D reconstruction from only basic geometrical constraints such as coplanarities or orthogonalities [25,26]. These methods represent geometrical constraints with non-linear equations that are solved using specialized algorithms. Compared to these systems, our method is much simpler.

3. System overview

As already described, we propose a laser scanning system that consists of a line laser projector and a fixed camera, which may be calibrated or uncalibrated, as shown in Fig. 1(left). First, we define several terms to describe geometrical elements that are used in this paper. Light projected by a line laser generates a plane in 3D space. We refer to this plane as a *laser plane*. When a scene is lit by a line laser, the intersection curves between the scene and the laser plane can be observed by a camera. We refer to these curves as *laser curves*. Some scenes include planar regions of surface. We refer to these regions as *explicit planes*.

In terms of line laser projector, various kinds of configuration can be considered. In this study, we actually constructed two types of configurations for our experiments. The first one is a single line laser projecting device, which is available easily with low cost (Fig. 2(a)). We call this configuration a *single-laser configuration*. We also built a special laser projecting device consisting of two line lasers that were aligned precisely at 90° as shown in Fig. 2(b). We call this configuration a *crosshair-laser configuration*. In this case, no metric constraints are required from the scene. The angle between the two laser planes can be adjusted by projecting the crosshair pattern to a plane on which a large pattern of an angle of 90° is drawn. This plane should be orthogonal to both of the laser planes. An example of methods to achieve this configuration, is using a corner of a rectangular room as shown in Fig. 2(c).

With the single-laser configuration, it is advantageous that no special device is needed for scanning 3D scenes. However there are some limitations for this configuration, such as that (1) explicit planes with some geometrical constraints such as orthogonalities between them are required in the scene, and that (2) user interactions are needed to specify the explicit planes and the geometrical constraints between them. With the crosshair-laser configuration, although a special laser projecting device is needed, explicit planes are not required in the target scenes, and thus, manual interactions are not necessary.

A scanning process of the system is performed as the following steps:

- Step 1 A sequence of images is captured with the fixed camera while moving the line laser back and forth manually.
- Step 2 While capturing, laser curves are extracted online and information of those extracted curves is stored instead of entire captured images to reduce data storage size.
- Step 3 From all the captured laser curves, a smaller number of laser curves are selected to reduce computational cost. For example, 20 to 40 frames with constant intervals were selected for our experiments.
- Step 4 By aggregating the selected laser curves on a common image plane, intersection points between those curves can be obtained. These intersection points are points that exist on multiple planes.
- Step 5 Applying the projective reconstruction method (Section 4), the laser planes of the selected laser curves are reconstructed up to 4-DOF indeterminacies from the coordinates of the intersection points on the image plane.
- Step 6 Then, 4-DOF indeterminacies are eliminated by applying the metric reconstruction method (Section 5) using metric constraints, such information is given by two ways:

Please cite this article in press as: R. Furukawa, H. Kawasaki, Laser range scanner based on self-calibration techniques using coplanarities and metric constraints, Comput. Vis. Image Understand. (2009), doi:10.1016/j.cviu.2009.05.006

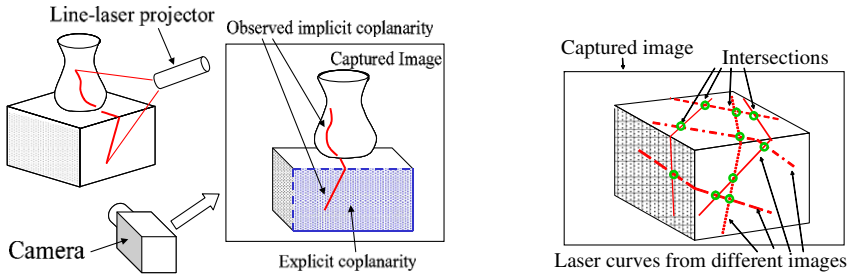

Fig. 1. (left) Observation of implicit and explicit coplanarities. (right) Points of intersection of the laser curves.

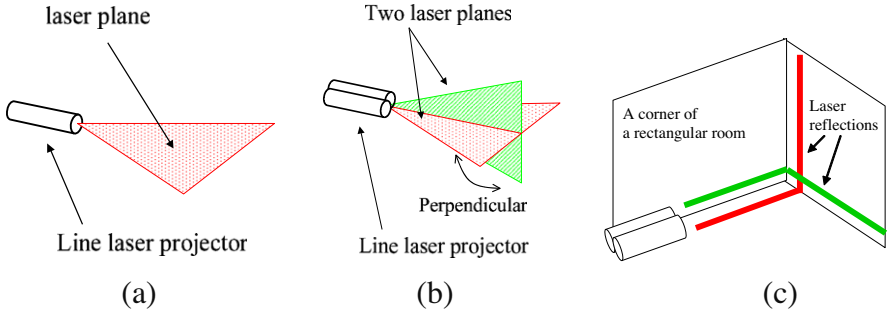

Fig. 2. Laser projecting device: (a) a laser projector with single-laser configuration, (b) a laser projector with crosshair-laser configuration, (c) a method for adjusting crosshair-laser configuration.

(a) For the single-laser configuration, this information can be retrieved from a scene manually. In terms of the manual step, drawing curves freely on a planar regions on an image, as shown in Fig. 3, is sufficient. It is easy and simple.
(b) For the crosshair-laser configuration, this information is automatically given from relationship between two lasers (90°).

Step 7 Using the reconstructed laser plane parameters and the extracted laser curves, 3D shapes of the selected laser curves are reconstructed by a *light-section method* (explained in Section 6).

Step 8 Using reconstruction results of the selected laser curves, laser curves from all the frames are reconstructed using the dense reconstruction technique (Section 6).

4. Projective reconstruction from coplanarities

Let us assume that we have a camera coordinate system whose origin is at the center of the perspective camera. The x and y axes are directed toward the right and top direction relative to the camera, respectively, and the z axis is directed backward from the camera. In this paper, the 3D coordinates are defined in the camera coordinate system.

Suppose a set of N planes including both laser planes and explicit planes (in the mathematical formulation, implicit and explicit coplanarities are treated equally in the proposed method). Let jth plane of the set be π_j. It is assumed that none of these planes includes the optical center of the camera.[1] Then, we can express the plane π_j by the form

$$a_j x + b_j y + c_j z + 1 = 0 \tag{1}$$

in the camera coordinates system.

[1] The reason is as follows. If a plane includes the optical center, the plane cannot be used to determine depths of the points on it because the length of baseline for triangulation is zero. Thus, the plane is not useful for 3D reconstruction and should be removed before projective reconstruction.

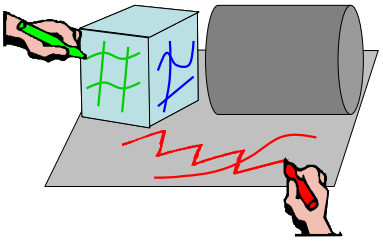

Fig. 3. Curves of each color are within a planar region and they are coplanar. Such coplanar curves are drawn by hand. (For interpretation of the references to colour in this figure legend, the reader is referred to the web version of this article.)

Suppose that we can observe M points that are on intersection lines of multiple laser planes or implicit planes as images of the points captured by a fixed camera. Let the ith point of the set be represented as ξ_i and exist on the intersection line of π_j and π_k. Let the coordinates $\mathbf{u}_i = [u_i, v_i]^\top$ be the image of ξ_i on the image plane. Let the 3D coordinates of ξ_i be $\mathbf{x}_i = [x_i, y_i, z_i]^\top$, let the upper triangular matrix that represents the intrinsic parameter of the camera be $\mathbf{K}$, and let $\tilde{\mathbf{u}}_i$ be defined as $\tilde{\mathbf{u}}_i \equiv [\mathbf{u}_i, 1]^\top$, then the projection of ξ_i can be represented as

$$z_i \begin{bmatrix} \mathbf{u}_i \\ 1 \end{bmatrix} = z_i \tilde{\mathbf{u}}_i = \mathbf{K}\mathbf{x}_i = \begin{bmatrix} \alpha & \sigma & p_u \\ 0 & \beta & p_v \\ 0 & 0 & 1 \end{bmatrix} \mathbf{x}_i, \tag{2}$$

where α, β, σ, p_u and p_v are intrinsic parameters of the camera. The objective of the problem is estimating the laser planes and the explicit planes from the 2D coordinates $\mathbf{u}_i$ ($1 \leqslant i \leqslant M$). The intrinsic parameters are also estimated if they are unknown.

Let the parameter vector of plane π_j be $\mathbf{a}_j = [a_j, b_j, c_j]^\top$. From the form (1),

$$\mathbf{a}_j^\top \mathbf{x}_i + 1 = z_i \mathbf{a}_j^\top \mathbf{K}^{-1} \tilde{\mathbf{u}}_i + 1 = z_i \mathbf{a}_j^{*\top} \tilde{\mathbf{u}}_i + 1 = 0, \tag{3}$$

where $\mathbf{a}_j^{*\top} = \mathbf{a}_j^\top \mathbf{K}^{-1}$. $\mathbf{a}_j^*$ can be regarded as a new parameter vector of plane π_j into which the intrinsic parameters are incorporated. In the

Please cite this article in press as: R. Furukawa, H. Kawasaki, Laser range scanner based on self-calibration techniques using coplanarities and metric constraints, Comput. Vis. Image Understand. (2009), doi:10.1016/j.cviu.2009.05.006

following, we describe a method to obtain $\mathbf{a}_j^*$. Dividing the form (3) by z_i and substituting $1/z_i$ with t_i,

$$\mathbf{a}_j^{*\top}\tilde{\mathbf{u}}_i + t_i = 0. \tag{4}$$

Since the point ξ_i is also on the plane π_k,

$$\mathbf{a}_k^{*\top}\tilde{\mathbf{u}}_i + t_i = 0 \tag{5}$$

Eq. (5) includes a variable t_i which depends on the depth of point ξ_i. In many cases, the number of the points, or M, becomes much larger than the number of planes, or N (for example, the data of Fig. 6(b) used in the experiment has 613 points, whereas there are only 40 planes). In these cases, using t_i as a variable causes a large increase of the number of variables, which is undesirable from the viewpoint of computational costs. So, we eliminate t_i from Eqs. (4) and (5). Then, a linear homogeneous equation

$$\tilde{\mathbf{u}}_i^\top\mathbf{a}_j^* - \tilde{\mathbf{u}}_i^\top\mathbf{a}_k^* = \tilde{\mathbf{u}}_i^\top(\mathbf{a}_j^* - \mathbf{a}_k^*) = 0 \tag{6}$$

with variables $\mathbf{a}_j^*$ and $\mathbf{a}_k^*$ can be obtained for each of the set of points. Since Eq. (6) is a homogeneous equation and only the difference $\mathbf{a}_j^* - \mathbf{a}_k^*$ appears in it, there are indeterminacies of scaling with a same factor and addition of a same vector. That is, if a set of variables $\mathbf{a}_j^* = \mathbf{a}_j'$ and $\mathbf{a}_k^* = \mathbf{a}_k'$ is a solution of Eq. (6) the set of

$$\mathbf{a}_j^* = s\mathbf{a}_j' + \mathbf{b}, \quad \mathbf{a}_k^* = s\mathbf{a}_k' + \mathbf{b} \tag{7}$$

is also a solution for an arbitrary scalar s and an arbitrary 3D vector $\mathbf{b}$.

The equations of form (6) for M points form a set of simultaneous homogeneous linear equations. This can be represented by a matrix $\mathbf{L}$ with M rows and $3N$ columns whose elements can be described by u_i, v_i $(1 \leqslant i \leqslant M)$, and a $3N$-dimensional solution vector $\mathbf{p} = \left[\mathbf{a}_1^{*\top}, \ldots, \mathbf{a}_N^{*\top}\right]^\top$. By using them, the equations can be described by a matrix form as

$$\mathbf{L}\mathbf{p} = 0. \tag{8}$$

The solutions of the form (8) have the same indeterminacies as the form (7). That is, if $\mathbf{p} \equiv \left[\mathbf{a}_1^{*\top}, \ldots, \mathbf{a}_N^{*\top}\right]^\top = \left[\mathbf{a}_1'^\top, \ldots, \mathbf{a}_N'^\top\right]^\top$ is a particular solution of Eq. (8),

$$\mathbf{p} \equiv \begin{bmatrix}\mathbf{a}_1^* \\ \vdots \\ \mathbf{a}_N^*\end{bmatrix} = \begin{bmatrix}s\mathbf{a}_1' + \mathbf{b} \\ \vdots \\ s\mathbf{a}_N' + \mathbf{b}\end{bmatrix} = s\begin{bmatrix}\mathbf{a}_1' \\ \vdots \\ \mathbf{a}_N'\end{bmatrix} + \begin{bmatrix}\mathbf{b} \\ \vdots \\ \mathbf{b}\end{bmatrix} \tag{9}$$

is also a solution for an arbitrary scalar s and an arbitrary 3D vector $\mathbf{b}$. Thus, the solution $\mathbf{p}$ has at least 4-DOF indeterminacy.

Here, we assume that the solutions of Eq. (8) have only the 4-DOF indeterminacy that is described above and degenerate conditions where this assumption does not hold will be discussed later. In this case, the general form of the solutions of Eq. (8) can be given as the form (9). Because of the indeterminacy of adding vector $[\mathbf{b}^\top, \ldots, \mathbf{b}^\top]^\top$, we can assume $\mathbf{a}_N' = 0$ for a particular solution $\left[\mathbf{a}_1'^\top, \ldots, \mathbf{a}_N'^\top\right]^\top$ without losing generality of the form (9). Under this assumption, by defining $\mathbf{p}' = \left[\mathbf{a}_1'^\top, \ldots, \mathbf{a}_{N-1}'^\top\right]^\top$ and by defining $\mathbf{L}'$ as the submatrix of the left $3N - 3$ columns of $\mathbf{L}$, we can get an equation $\mathbf{L}'\mathbf{p}' = 0$. Then, $\mathbf{p}'$ can be obtained as the basis of the 1-D null space of $\mathbf{L}'$, and the general solution $\mathbf{p}$ can be represented by

$$\mathbf{p} \equiv \begin{bmatrix}\mathbf{a}_1^* \\ \vdots \\ \mathbf{a}_N^*\end{bmatrix} = s\begin{bmatrix}\mathbf{p}' \\ 0\end{bmatrix} + \begin{bmatrix}\mathbf{b} \\ \vdots \\ \mathbf{b}\end{bmatrix} \equiv s\begin{bmatrix}\mathbf{a}_1' \\ \vdots \\ \mathbf{a}_{N-1}' \\ 0\end{bmatrix} + \begin{bmatrix}\mathbf{b} \\ \vdots \\ \mathbf{b}\end{bmatrix} \tag{10}$$

using an arbitrary scalar s and an arbitrary 3D vector $\mathbf{b}$.

In real data, observation noise is included. Even in these cases, Eq. (8) has a trivial solution $\mathbf{p} = 0$. Also, because of the form of Eq. (6), the 3-DOF indeterminacy caused by a vector $\mathbf{b}$ rigorously remains even if the data has observation noise. The 3-DOF indeterminacy caused by a scalar s does not rigorously remains for real data. Thus, for actual data that has noise and is not a degenerate condition, $\mathbf{L}$ has three zero singular values and one small singular value (the fourth minimum singular value). From the same reason, $\mathbf{L}'$ does not have a rigorous null space, but its minimum singular value becomes small.

To conclude this section, we point out that the 4-DOF indeterminacy of the general solution of the planes can be described as 4-parameter 3D homographies that transform the 3D points and the plane parameters. The plane parameter $\mathbf{a}_j^{*\top}$ can be described as a 3D homogeneous coordinates $\left[\mathbf{a}_j^{*\top}\ 1\right]^\top$. Let a 4×4 matrix $\mathbf{B}(\mathbf{b}, s)$ be defined as

$$\mathbf{B}(\mathbf{b}, s) = \begin{bmatrix}s\mathbf{I} & 0 \\ \mathbf{b}^\top & 1\end{bmatrix}. \tag{11}$$

Because of the indeterminacy described as the form (9), if a set of planes $\left[\mathbf{a}_j^{*\top}\ 1\right]\top,\ 1 \leqslant j \leqslant N$ is a solution, then the set of planes

$$\left[\mathbf{a}_j^{*\top}\ 1\right]\mathbf{B}(\mathbf{b}, s), \quad l \leqslant j \leqslant N \tag{12}$$

is also a solution.

The plane parameter $\mathbf{a}_j^* = \mathbf{K}^{-1}\mathbf{a}^*$ can be regarded as a projective plane that is transformed by the intrinsic parameters of the camera. Let a point on the projective plane $\mathbf{a}_j^*$ be $\mathbf{x}^*$, then, $\mathbf{a}_j^{*\top}\mathbf{x}^* = 0$. Since the inverse of $\mathbf{B}(\mathbf{b}, s)$ is $(\mathbf{B}(\mathbf{b}, s))^{-1} = \mathbf{B}(-(1/s)\mathbf{b}, 1/s)$,

$$\left[\mathbf{a}_j^{*\top}\ 1\right]\begin{bmatrix}\mathbf{x}^* \\ 1\end{bmatrix} = 0 \Rightarrow \left\{\left[\mathbf{a}_j^{*\top}\ 1\right]\mathbf{B}(\mathbf{b}, s)\right\}\left(\mathbf{B}(-(1/s)\mathbf{b}, 1/s)\begin{bmatrix}\mathbf{x}^* \\ 1\end{bmatrix}\right) = 0 \tag{13}$$

holds. These forms mean that, if a plane parameter is transformed by the form (12), points on the plane $\mathbf{x}^*$ are transformed by the homography $\mathbf{B}(-(1/s)\mathbf{b}, 1/s)$. This form represents a group of 4-parameter homographies that transform 3D points $\mathbf{x}^*$ and are called generalized projective bas-relief transformations [27]. It is also pointed out in Ref. [28] that solutions of shape reconstruction using line-lasers or shadows of straight edges inevitably have 4-DOF indeterminacy unless using some metric constraints.

Note that, for the crosshair-laser configuration, we do not have to distinguish the cross points formed by the two laser lines of crosshair pattern and other intersection points. This is because the two laser planes generated by the projector can be treated as unrelated two planes in projective reconstruction step. The orthogonality between those two planes is used in metric reconstruction step described in Section 5.

4.1. Degenerate conditions

To obtain the solution of form (10), it is assumed that the degrees of freedom of solution $\mathbf{p}$ of Eq. (8) is four. Here, we discuss the conditions under which this assumption holds true. We have assumed that there are N planes in the scene, thus, the number of parameters of the planes is $3N$. Since one intersection point yields one equation, at least $3N - 4$ points are required for the solution having 4-DOF indeterminacy. However, even if this condition is fulfilled, the solution may have indeterminacy of more degrees of freedom, because of degenerate conditions caused by the specific locations of the points or the specific shape of the scene. In the following are examples of such cases.

Fig. 4(a) shows extracted laser curves drawn as bold solid curves and a single dashed curve. In the figure, "all" the intersection points (circles in the figure) between the dashed laser curve and the others (solid curves) are on a single line (*i.e.*, collinear). In this case, the laser plane that includes the dashed laser curve has indeterminacy even if all the other curves are determined.

Please cite this article in press as: R. Furukawa, H. Kawasaki, Laser range scanner based on self-calibration techniques using coplanarities and metric constraints, Comput. Vis. Image Understand. (2009), doi:10.1016/j.cviu.2009.05.006

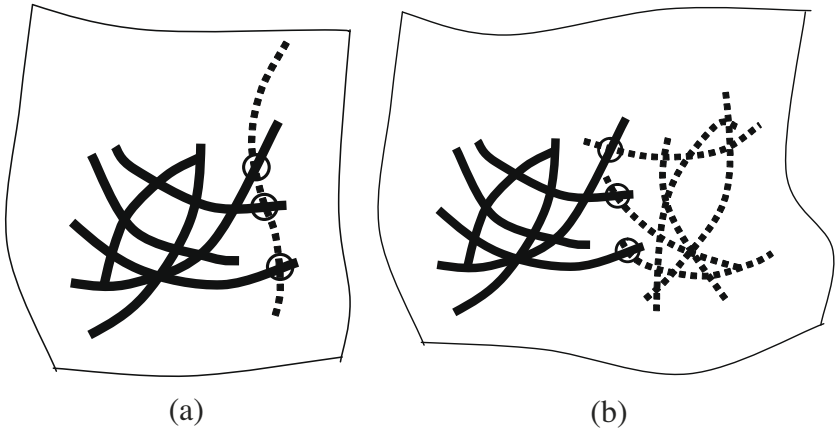

Fig. 4. Examples of solutions having more than 4-DOF indeterminacy.

Thus, it is a degenerate condition and the total indeterminacy is more than 4 DOFs. This case often occurs if the target scene includes planar regions. Since the laser curve becomes a straight line segment in a planar region, the collinear condition is fulfilled if all the intersection points of a laser curve is in a planar region. Thus, this type of degenerate conditions often occurs, and it is desirable to detect such laser curves and remove them. A method for achieving this is described later.

In contrast to a degenerate condition of Fig. 4(a) caused by a single laser curve, there are also degenerate conditions caused by multiple laser curves. Since the number of combinations of multiple laser curves is large, general discussion of the conditions is not easy. However, it is possible to show some examples. Fig. 4(b) is such an example, where the set of laser curves are divided into either solid curves or dashed curves, and "all" the intersection points (circles in the figure) between those two groups are collinear on the image plane. In this case, the shapes of the dashed laser curves have indeterminacy, even if all the shapes of the solid curves are determined, and the total indeterminacy is more than 4 DOFs. Since this condition requires special arrangements of the laser curves, it seldom occurs if sufficiently large number of laser curves are captured.

There is a simple method which we have found effective for reducing degenerate conditions shown in Fig. 4(a). For each laser curve, collinearity of the set of intersection points that are on the curve should be checked. If they are collinear, the laser curve is not used for reconstruction. Obviously, the cases of Fig. 4(a) are avoided by this method. A method for detecting collinearity from real data is based on principal component analysis. If the root of variance of the second component of the intersection points of a laser curve is less than a threshold, these points are determined to be collinear. In actual cases, numerical stability of the projective solution often becomes worse even if those intersection points are just "nearly collinear." To avoid these near collinearity, using a "large" threshold (*e.g.*, about 10 pixels) is a practical solution.[2] If we apply this method to the target scene that has 3D shape (*i.e.*, not a planar scene) and the number of the detected laser curves are sufficiently large and all of them are "connected" (*i.e.*, not divided into multiple sets that are not connected with each other), then, our experience suggests that the assumption of 4-DOF indeterminacy is fulfilled in most of the cases.

Even if the above method is used, degenerate conditions may occur, in case of, for example, Fig. 4(b). Such cases can be detected by observing the rank of matrix **L**. If the rank of **L** is less than $3N-4$, we can just estimate more unknown parameters at the metric reconstruction step using the non-linear method. Thus, it does not severely affect the result.

If **L** is generated from a real data, the rank of the matrix with no degenerate condition does not becomes $3N-4$ rigorously because of the observation errors, as described after Eq. (10). To detect degenerate conditions from a real data, counting singular values of **L** that are less than a threshold is one practical solution.[3]

5. Metric reconstruction

As described in the previous section, the solutions of the plane parameters $\mathbf{a}_j^*,\ j=1,\ldots,N$ of the form (10) have 4-DOF indeterminacy which include 1-DOF indeterminacy of scaling. Moreover, if any of the intrinsic parameters are unknown, $\mathbf{a}_j^*,\ j=1,\ldots,N$ include variables of the parameters which cause additional indeterminacy.

These indeterminacies cannot be reduced using coplanarities. If metric constraints are available, we may reduce the indeterminacies using these constraints. For example, if only the focal length is unknown within the intrinsic parameters, and if we need the shape of the scene up to scale from orthogonalities in the scene,[4] the number of required metric constraints is at least 4 + 1 (number of DOF for focal length) − 1 (number of DOF for scaling) = 4 + 1 − 1 = 4.

5.1. Linear method

If we have many (at least nine) orthogonalities between planes as metric constraints, it is possible to achieve metric reconstruction up to scale estimating all the intrinsic parameters using a linear method. From the definition in Eq. (4), $\mathbf{a}_j^{*\top}=\mathbf{a}_j^{\top}\mathbf{K}^{-1}$. Thus, the plane parameter $\mathbf{a}_j^{\top}$ in the Euclidean space can be represented as

[2] This method is also effective for removing laser curve generated by a laser plane that includes the optical center of the camera, which violates the assumption of the planes described in Section 4, because a laser curve generated by such a plane becomes a straight line in captured images.

[3] How to determine a good threshold is one of the future works. In actual cases, the number of optimized parameters of non-linear optimization can be larger than the actual number of free parameters. Although there are costs of a wider search space and requiring more metric conditions (metric conditions are described in Section 5), correct solution can be obtained even if a larger number of parameters are optimized. Thus, one approach for this problem may be using a large threshold.

[4] The kind of indeterminacies that are reducible depends on the kind of metric constraints. For example, indeterminacy of scaling is not reducible using orthogonalities or parallelisms in the scene.

Please cite this article in press as: R. Furukawa, H. Kawasaki, Laser range scanner based on self-calibration techniques using coplanarities and metric constraints, Comput. Vis. Image Understand. (2009), doi:10.1016/j.cviu.2009.05.006

$$\mathbf{a}_j^\top = \mathbf{a}_j^{*\top}\mathbf{K} = \left(s\mathbf{a}'_j + \mathbf{b}\right)^\top \mathbf{K}, \quad j = l, \ldots, N \tag{14}$$

using an arbitrary scalar s and an arbitrary 3D vector $\mathbf{b}$. The scalar s corresponds to scaling in the Euclidean space, which cannot be determined from only orthogonalities of planes in principle. So, $s = 1$ is assumed. Then, the condition of orthogonality between π_j and π_k can be represented as

$$\begin{aligned}\mathbf{a}_j^\top \mathbf{a}_k &= \left(\mathbf{a}_j'^\top + \mathbf{b}^\top\right)\mathbf{K}\mathbf{K}^\top\left(\mathbf{a}'_k + \mathbf{b}\right) = \begin{bmatrix}1 & \mathbf{a}_j'^\top\end{bmatrix}\begin{bmatrix}\mathbf{b}^\top\mathbf{K} \\ \mathbf{K}\end{bmatrix}\begin{bmatrix}\mathbf{K}^\top\mathbf{b} & \mathbf{K}^\top\end{bmatrix}\begin{bmatrix}1 \\ \mathbf{a}'_k\end{bmatrix} \\ &= \begin{bmatrix}1 & \mathbf{a}_j'^\top\end{bmatrix}\mathbf{Q}\begin{bmatrix}1 \\ \mathbf{a}'_k\end{bmatrix} = 0\end{aligned} \tag{15}$$

where $\mathbf{Q}$ is a 4×4 symmetric matrix defined as

$$\mathbf{Q} = \begin{bmatrix}\mathbf{b}^\top\mathbf{K} \\ \mathbf{K}\end{bmatrix}\begin{bmatrix}\mathbf{K}^\top\mathbf{b} & \mathbf{K}^\top\end{bmatrix} = \begin{bmatrix}\mathbf{b}^\top\mathbf{K}\mathbf{K}^\top\mathbf{b} & \mathbf{b}^\top\mathbf{K}\mathbf{K}^\top \\ \mathbf{K}\mathbf{K}^\top\mathbf{b} & \mathbf{K}\mathbf{K}^\top\end{bmatrix}. \tag{16}$$

The form (15) can be regarded as a linear equation with respect to the elements of $\mathbf{Q}$. Considering that $\mathbf{Q}$ is a 4×4 symmetric matrix which has ten distinct elements and that the right-bottom element of $\mathbf{Q}$ is always 1, nine elements should be determined (note that this number of unknown elements (=9) equals to the sum of the number of unknown elements of $\mathbf{K}$ (=5) and the number of unknown parameters of a generalized projective bas-relief transformation (=4)). If we have nine independent conditions of orthogonalities, we can determine $\mathbf{Q}$. Since the right-bottom 3×3 submatrix of $\mathbf{Q}$ is $\mathbf{K}\mathbf{K}^\top$, $\mathbf{K}$ can be determined by Cholesky factorization of the submatrix. Once $\mathbf{K}$ is determined, $\mathbf{b}$ can be calculated by $\mathbf{b} = (\mathbf{K}\mathbf{K}^\top)^{-1}\mathbf{q}$, where $\mathbf{q}$ is the left-bottom 3×1 submatrix of $\mathbf{Q}$.

5.2. Non-linear method

The linear method described in Section 5.1 can be used without initial solutions, however, it can be applied only if at least nine orthogonalities between laser/explicit planes are available. Even if it is true, these conditions are often dependent or nearly dependent with each other. In these cases, the linear method tends to be unstable.

In real situations, some or all of the intrinsic parameters may be known. In these cases, it is often effective to achieve metric reconstruction by minimization of an error function that is defined to have the minimum value if the metric constraints are fulfilled. In the proposed method, the plane parameter $\mathbf{a}_j$ in the Euclidean space is described using a set of unknown parameters of the intrinsic parameters, which is represented as Θ, and variables s and $\mathbf{b}$ of the form (10). Let this representation be described as $\mathbf{a}_j(\Theta, s, \mathbf{b})$. Then, for example, if we have a set of conditions of orthogonalities from the scene, which is represented as a set of pairs of indices of planes that are orthogonal, $C_v = \{(i,j)|(\pi_i \perp \pi_j)\}$, we can define an error function $E(\mathbf{b}, \Theta)$ as

$$\begin{aligned}E(\mathbf{b}, \Theta) &= \sum_{(i,j)\in C_v} \cos^2\theta_{ij}(\mathbf{b}, 1, \Theta) \\ &= \sum_{(i,j)\in C_v} \{N(\mathbf{a}_i(\mathbf{b}, 1, \Theta))^\top N(\mathbf{a}_j(\mathbf{b}, 1, \Theta))\}^2,\end{aligned} \tag{17}$$

where $\theta_{ij}(\Theta, s, \mathbf{b})$ is the angle between the planes π_i and π_j, and $N(\,)$ means normalization of a vector. $E(\mathbf{b}, \Theta)$ does not have s as an argument because the scaling cannot be determined from only orthogonalities. Using the error function, we can obtain estimations of $\mathbf{b}$ and Θ, which are depicted as $\hat{\mathbf{b}}$ and $\widehat{\Theta}$, by solving the non-linear optimization problem of

$$(\hat{\mathbf{b}}, \widehat{\Theta}) = \arg\min_{(\mathbf{b},\Theta)} E(\mathbf{b}, \Theta). \tag{18}$$

Achieving metric reconstruction using non-linear optimization has an advantage that the kinds of usable metric constraints can be easily increased by representing new constraints as error functions. For example, if parallelisms of planes are available as a set $C_p = \{(i,j)|\pi_i$ and π_j are parallel$\}$ in addition to orthogonalities of planes, the error function can be defined as

$$\begin{aligned}E(\mathbf{b}, \Theta) &\equiv \sum_{(i,j)\in C_v} \cos^2\theta_{ij}(\mathbf{b}, 1, \Theta) + \sum_{(i,j)\in C_p} \sin^2\theta_{ij}(\mathbf{b}, 1, \Theta) \\ &= \sum_{(i,j)\in C_v} \{N(\mathbf{a}_i(\mathbf{b}, 1, \Theta))^\top N(\mathbf{a}_j(\mathbf{b}, 1, \Theta))\}^2 \\ &\quad + \sum_{(i,j)\in C_p} \|N(\mathbf{a}_i(\mathbf{b}, 1, \Theta)) \times N(\mathbf{a}_j(\mathbf{b}, 1, \Theta))\|^2.\end{aligned} \tag{19}$$

Other types of metric constraints can be used as long as they can be represented as an equation described by using $\hat{\mathbf{b}}$, s, $\widehat{\Theta}$, or constant values.

Many methods have been proposed for non-linear optimization. We used an implementation of Levenberg–Marquardt method in the experiments described later.

For non-linear optimization, determining initial values is sometimes a problem. In the experiments, orthogonal projections of planes with manually entered parameters into the solution spaces of the form (10), which can be represented as $3N$-dimensional linear spaces, were calculated, and the projections were used as the initial solutions.

6. Dense 3D shape reconstruction

The above-mentioned method is only applied to selected laser curves, and results in a sparse 3D reconstruction. In order to obtain a dense 3D shape, we need to reconstruct all the laser curves (dense reconstruction). To achieve this, we first estimate the parameters of each selected laser plane, and then reconstruct all the 3D points on the selected laser curves by applying triangulation. This triangulation can be conducted by calculating the intersection between the laser plane and the line of sight which goes through the point on a detected laser curves as shown in Fig. 5. This method is generally called a light-section method. The actual process of the dense reconstruction is as follows:

Step 1 Up to this point, only the laser plane parameters of the selected frames are estimated using the aforementioned method. Thus, recover all the 3D positions of the points on the laser curves by using the estimated plane parameters and a light-section method.

Step 2 Detect the intersections between a laser curve on an arbitrary frame and the selected laser curves that have already been reconstructed in step 1.

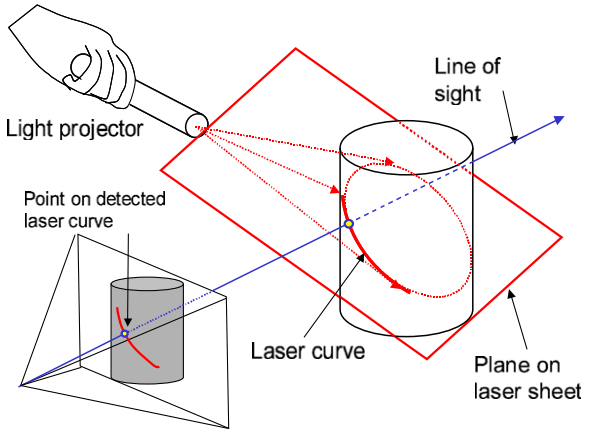

Fig. 5. Light-section method.

Please cite this article in press as: R. Furukawa, H. Kawasaki, Laser range scanner based on self-calibration techniques using coplanarities and metric constraints, Comput. Vis. Image Understand. (2009), doi:10.1016/j.cviu.2009.05.006

Step 3 Estimate the plane parameters of the laser curve on the frame processed in step 2 by fitting the intersection points to a plane by using principal components analysis.
Step 4 Recover all the 3D positions of the points on the laser curve by using the estimated plane parameters from step 3.
Step 5 Iterate steps 2–4 for all the frames until all the detected laser curves are reconstructed.

7. Experiments

7.1. Reconstruction from implicit coplanarities in a CG synthesized scene

We performed an experiment on the reconstruction of general scenes from the laser curves observed by a camera. To obtain the metric constraints, we assumed a laser projector composed of two line lasers, whose laser planes are configured to be perpendicular as described in Section 3. Using the device, the scene can be reconstructed without any metric constraints from the scene itself. In the experiments, the metric constraints are solved by both the linear method described in Section 5.1 and the non-linear method described in Section 5.2. For the non-linear method, we used the Levenberg–Marquardt method for optimizations. All the algorithms were implemented using C++ programming language.

Fig. 6(a) shows the data synthesized using CG. The purpose of this experiment was validating the reconstruction algorithms themselves, and not validating the steps for extracting intersection points. Thus, the laser curves are rendered to CG images as borders between black and white regions as shown in Fig. 6(b) and the curves are extracted in sub-pixel accuracy using marching squares algorithm (2D version of marching cubes algorithm). The size of the CG image was 800×600.

The scene shows a model of a rabbit. For this scene, the cross-sections of the laser planes and the model were rendered for various positions of the laser projector. The borders of the black and white patterns on the scene represent the cross-sections. The images are taken 20 times, and 40 laser planes exist in the scene. The metric constraints are 20 orthogonalities between the planes.

For the experiment of linear method, all the intrinsic parameters ($\alpha, \beta, \sigma, p_u$ and p_v) were estimated. For the non-linear method, we assumed $\alpha/\beta = 1$, $p_u = p_v = 0$ for the intrinsic parameters and estimated the value of α. To obtain the initial solution for the non-linear optimization, all the planes were manually classified into four categories based on their normal directions, and the initial parameters for each plane are decided based only on the categories. For example, the initial solutions of the planes of the "downward" category were decided as $z = 0x + 1y - 1$. Then, the metric reconstruction was calculated as described in Section 5.2. For the reconstruction, 588 intersection points were used. For the reconstruction, 588 intersection points were detected by calculating intersections between the laser curves with sub-pixel accuracy. The processing time for the projective reconstruction was 0.047 s

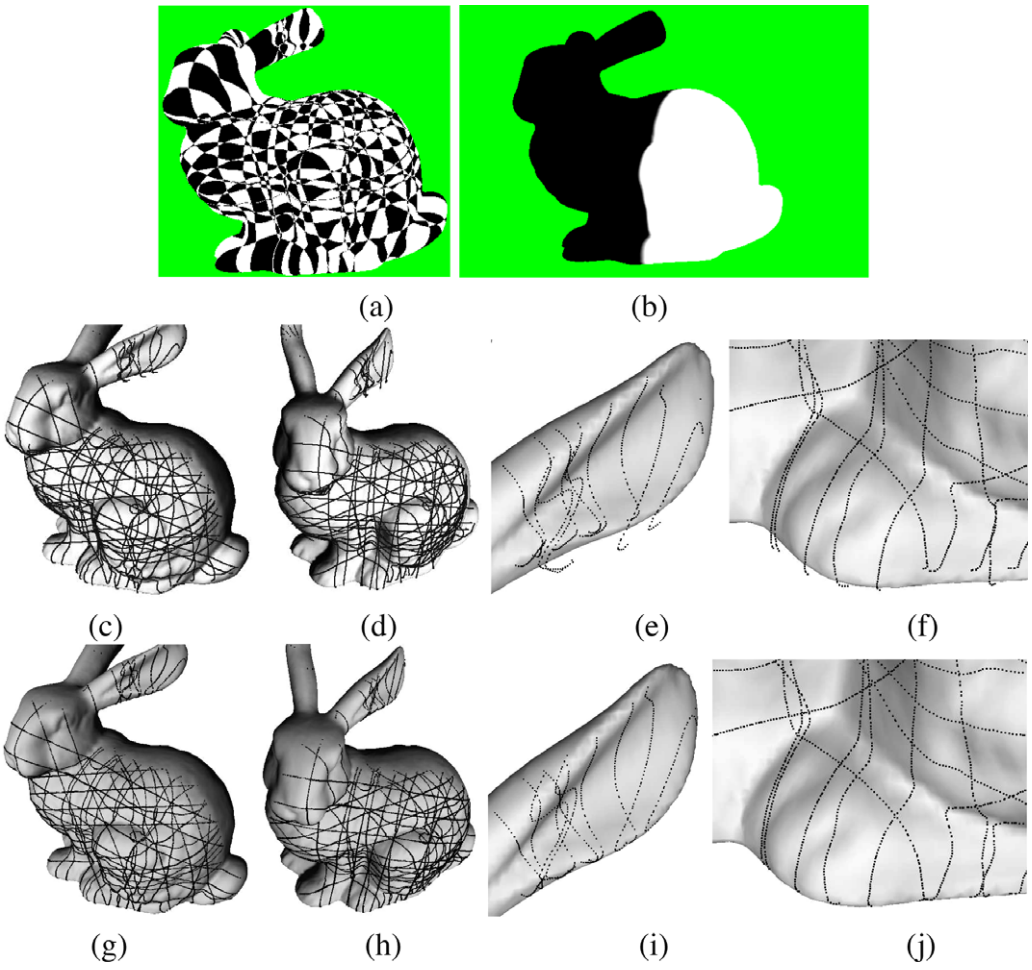

Fig. 6. Reconstruction of a CG-synthesized scene: (a) the laser curves, (b) a example of laser curve rendered in CG image, (c)–(f) the result of linear method, and (g)–(j) the result of non-linear method. (e), (f), (i) and (j) are zoomed-in views of one of the ears and the bottom. In (c)–(j), the dark curves or points are the reconstructed laser curves and the shaded surfaces are the ground truth models.

Please cite this article in press as: R. Furukawa, H. Kawasaki, Laser range scanner based on self-calibration techniques using coplanarities and metric constraints, Comput. Vis. Image Understand. (2009), doi:10.1016/j.cviu.2009.05.006

(it does not include the time for extracting intersection points). The processing times for non-linear and linear method for metric reconstruction were 0.015 s and 0.016 s, respectively. These processing time were measured on a PC with a Pentium Xeon 3.8 GHz CPU. The same system was used for all the following experiments.

Since the scaling factor cannot be solved, we scaled the solution using the ground truth solution for evaluation. Fig. 6(b)–(e) shows the scaled solution of the linear method (the estimated laser curves) with the shaded ground truth model, and (f)–(i) show that of the non-linear method. The figures show that the result of the non-linear method is better than that of the linear method. A part of the reason is that the linear method also estimates the camera model, which is not estimated in the non-linear method. By the linear method, $(\alpha, \alpha/\beta, \sigma, p_u, p_v)$ were calculated to be $(7.560 \times 10^2, 0.999570, 0.808, -3.57, -2.15)$, whereas their true values were $(7.464 \times 10^2, 1, 0, 0, 0)$. The units of p_u and p_v were pixels and the size of the image was 600×400. By the non-linear method, α was calculated to be 7.467×10^2. To estimate the error of the reconstruction quantitatively, we calculated the RMS error of the z-coordinates of all the reconstructed points where the average of the z-coordinates of the points was scaled to 1.0 (*i.e.*, normalized by the average of the z-coordinates). The RMS error was 7.543×10^{-3} for the linear method and 4.822×10^{-5} for the non-linear method.

7.2. Reconstruction from implicit coplanarities in real scenes

To conduct experiments for a real object, we use a system consisting of a line laser projector and a video camera as described in Section 3.

In the first experiment, we used the single-laser configuration. We selected 20 images from a captured image sequence and reconstructed the 3D shape. There were two rectangular boxes in the target scene as shown in Fig. 7(a). Fig. 7(b) shows an example of the selected images. From the images, the laser curves captured by the camera were extracted, and the regions of 6 faces of the boxes were also extracted as explicit planes manually. Detection of laser curves was conducted by thresholding the pixel values of the red channel and the green channel. Then, pixels that were shared by multiple laser curves were detected. Since laser curves were not skeletonized, each of the intersection points corresponded to multiple pixels. Thus, each of the connected regions was extracted as an intersection point, whose position was calculated as the center of gravity of the region. For projective reconstruction, 151 intersection points were used and 13 orthogonalities between the explicit planes were used for metric reconstruction. 101,339 points were reconstructed in the dense reconstruction process. Fig. 7(c)–(f) shows the extracted laser curves and the reconstruction results. The processing time was 0.015 s for projective reconstruction, 0.016 s for metric reconstruc-

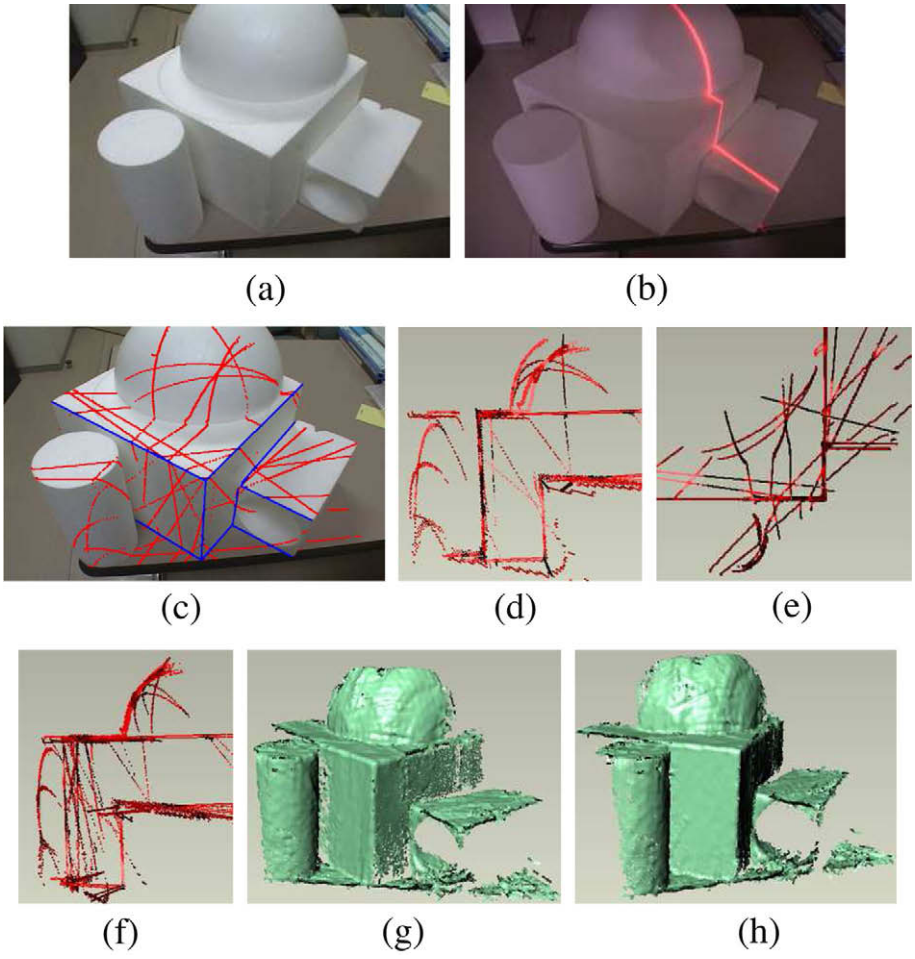

Fig. 7. Reconstruction of the real scene: (a) the target scene, (b) the laser curves, (c) extracted reflections (red curves) and explicit coplanarities (blue lines); (d)–(f) reconstructed scene of line-lasers; and (g) and (h) dense reconstruction. (For interpretation of the references to colour in this figure legend, the reader is referred to the web version of this article.)

Please cite this article in press as: R. Furukawa, H. Kawasaki, Laser range scanner based on self-calibration techniques using coplanarities and metric constraints, Comput. Vis. Image Understand. (2009), doi:10.1016/j.cviu.2009.05.006

tion, and 0.62 s for dense reconstruction for 3900 frames. We can clearly see that the orthogonalities of the rectangular box and the parallelisms of the edges were successfully reconstructed. Fig. 7(g) and (h) shows the dense 3D reconstruction result. We can confirm that a dense reconstruction was successfully achieved.

Next, we used a laser projecting device that emits two laser planes that are orthogonal with each other (the crosshair-laser configuration). In this case, no metric constraints were required from the scene. We selected 23 images and reconstructed the 3D shape. We also conducted a dense reconstruction. Image processing for detecting the laser curves and the intersection points were the same as the previous experiment. Fig. 8(a)–(g) shows all the inputs and results. We used 43 laser curves (3 lines were removed because intersection points on each of those lines were collinear as described in Section 4.1) with 975 intersection points for projective reconstruction, and used 20 orthogonalities for metric reconstruction. 213,437 points were reconstructed in the dense reconstruction process. The processing time was 0.078 s for projective reconstruction and 0.016 s for metric reconstruction, and 0.37 s for dense reconstruction for 2160 frames. We can see that an arbitrary shape was successfully reconstructed.

About the overall processing time for the system, the image capturing process takes about 1 min. For the single-laser configuration, it takes about several minutes to manually input information of explicit planes (drawing curves on regions as Fig. 3 and specifying metric constraints such as orthogonalities). Specifying initial estimations of the planes also takes several minutes. Thus the total processing time is about 10–20 min.

For the crosshair-laser configuration, specifying explicit planes are not needed. For such a system, it is also possible to give initial estimations of the planes by limiting the pose of the laser-projecting device while capturing by displaying "hints" of how to wave the laser projecting device. In this case, the system can reconstruct 3D shape online.

Next, an example of detection of a degenerate condition of Fig. 4 is shown. Fig. 9(a) shows a scene with a rectangular box, and (b) and (c) show images with laser curves generated by a projector with the crosshair-laser configuration. Because one of the laser curves in Fig. 9(c) existed mostly on a planar region, intersection points on the curve became nearly collinear. This caused a degenerate condition and reconstruction failed to produce an almost flat shape when this laser curve was included in the data. However, this curve could be detected by principal component analysis that is described in Section 4.1. By removing the curve, reconstruction succeeded as shown in Fig. 9(e) and (f).

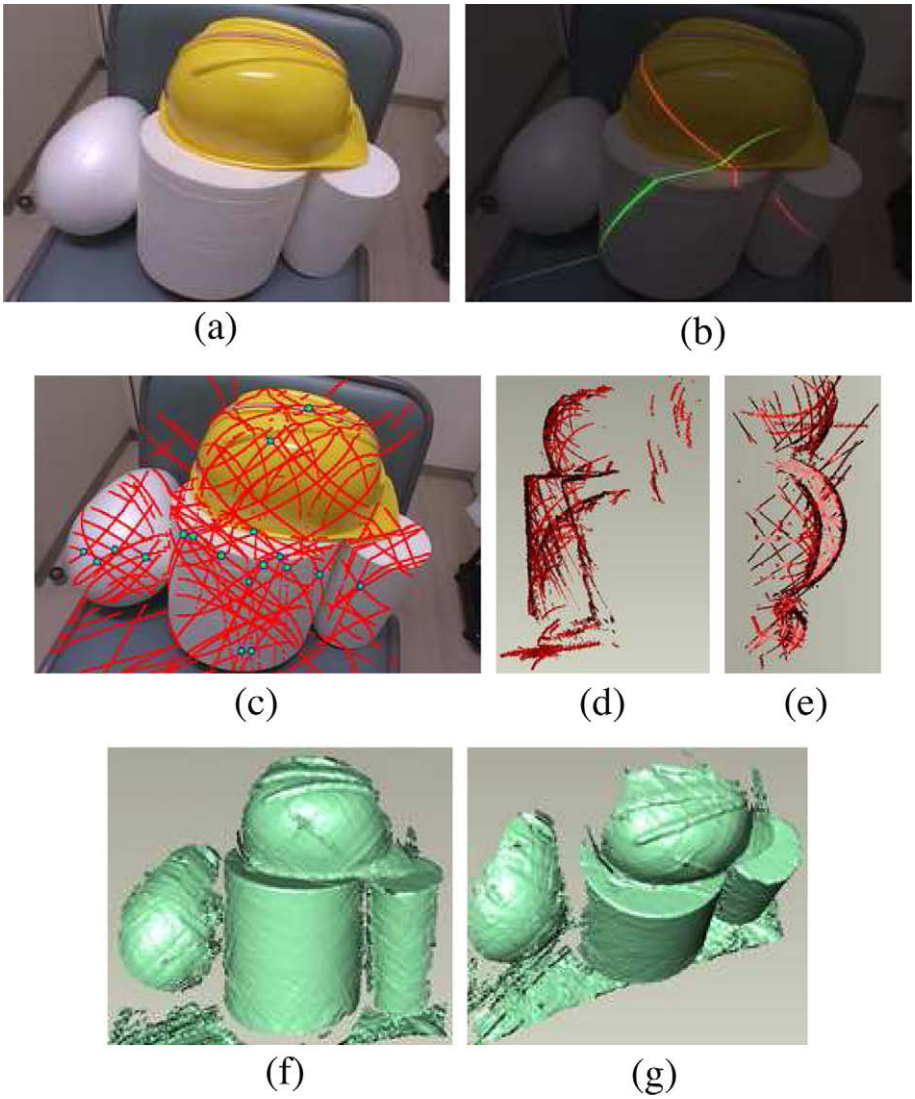

Fig. 8. Another result of real scene reconstruction with the crosshair-laser configuration.

Please cite this article in press as: R. Furukawa, H. Kawasaki, Laser range scanner based on self-calibration techniques using coplanarities and metric constraints, Comput. Vis. Image Understand. (2009), doi:10.1016/j.cviu.2009.05.006

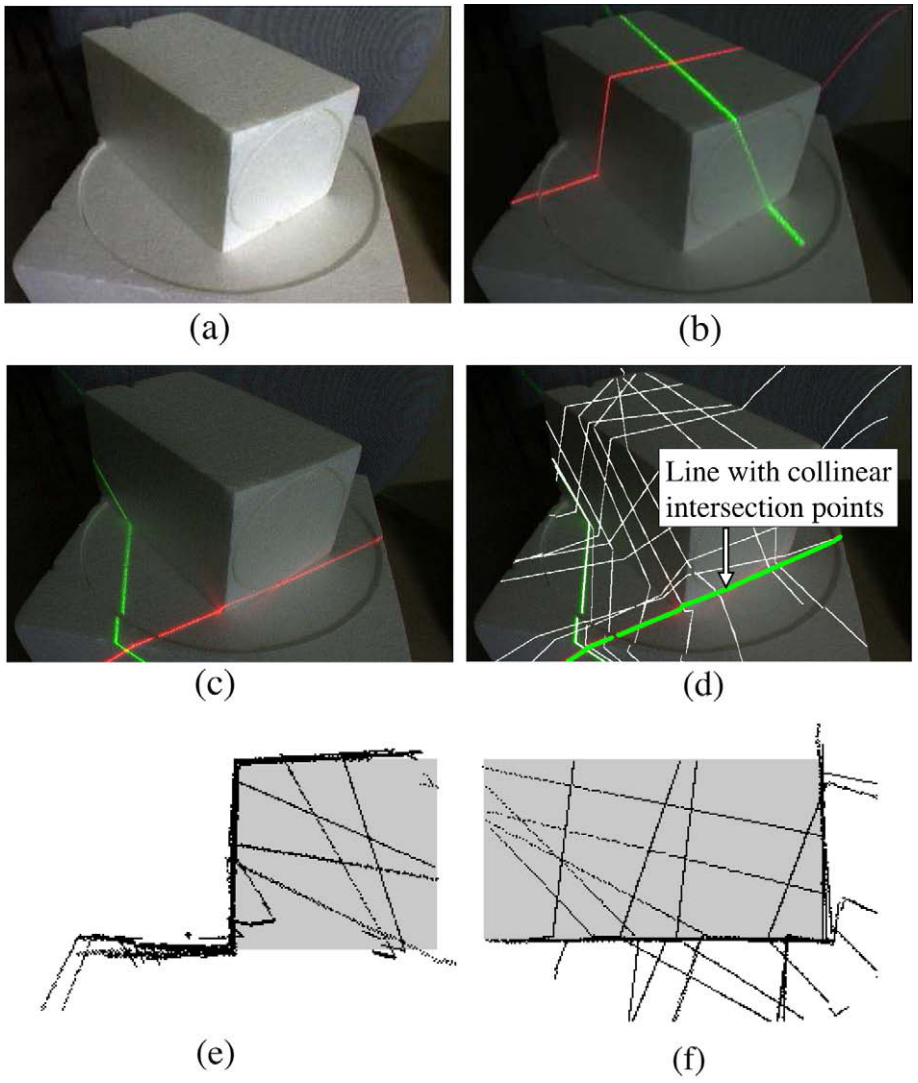

Fig. 9. An example of detection of degenerate conditions: (a) the target scene, (b) a captured image, (c) a captured image that causes a degenerate condition, (d) accumulated laser curves, and (e) and (f) the side and top views of the reconstructed points (sparse curves).

7.3. Reconstruction from single images

To confirm that the proposed method can be applied for single view reconstruction without implicit coplanarities, we reconstruct 3D shapes of two scenes. The first one includes the metric constraints assumed in conventional reconstruction methods, such as pairs of vanishing points whose directions are perpendicular. The second one does not include such specific constraints.

Fig. 10(a) shows the image used in the first experiment. The camera parameters of this image was unknown. From the scene, we extracted coplanarities and orthogonalities. The scene reconstruction and estimation of the intrinsic parameters were performed for the image. The Euclidean reconstruction was performed assuming $\alpha = \beta$, $\sigma = 0$, $p_u = p_v = 0$. The reconstruction was performed up to scale. Fig. 10(b) and (c) shows the result of the Euclidean reconstruction. The 3D scene was properly reconstructed, including the orthogonalities and parallelisms.

Next, we synthesized and reconstructed a CG image of a scene that included two columns as shown in Fig. 11(a), and the reconstruction was performed for the image. The shapes of the columns are long rectangular boxes. The tops of these boxes are invisible and the bottoms are occluded by the floor. By using vertices $A, B, \ldots$, and R shown in Fig. 11(a), the projective reconstruction of the five planes of the scene (the floor and the 4 faces of the 2 columns) were obtained.

There are two parallelisms in the scene, but the angle between the directions of the parallel lines is unknown. Moreover, neither rectangular boxes nor parallelepiped shapes exist in the scene. Therefore, reconstruction methods that assume such features are not applicable for this scene. However, the scene does include a sufficient number of metric constraints such as two orthogonalities of the planes of the columns (orthogonalities between faces *ABKJ* and *BCLK*, and between faces *DEHG* and *EFIH*), two known ratios of the short edges ($d_1/d_2 = d_4/d_3 = 1.3$, where d_1, d_2, d_3 and d_4 are the distances between lines *AJ* and *BK*, between lines *BK* and *CL*, between lines *DG* and *EH*, and between lines *EH* and *FI*, respectively), and two parallelisms along the two columns (parallelisms between lines *AJ, BK* and *CL*, and between lines *DG, EH* and *FI*); thus, our method is applicable. We performed Euclidean reconstruction up to scale and estimated α, assuming $\alpha = \beta$, $\sigma = 0$, $p_u = p_v = 0$. The result of the reconstruction is shown in Fig. 11(b)–(e). α was calculated to be 1.101×10^3, whereas its true value is 1.120×10^3. We can see that the scene was properly reconstructed and α was correctly estimated. The RMS of the error ratio of the reconstructed points calculated in the same way as the previous experiment was 1.990×10^{-3}.

Please cite this article in press as: R. Furukawa, H. Kawasaki, Laser range scanner based on self-calibration techniques using coplanarities and metric constraints, Comput. Vis. Image Understand. (2009), doi:10.1016/j.cviu.2009.05.006

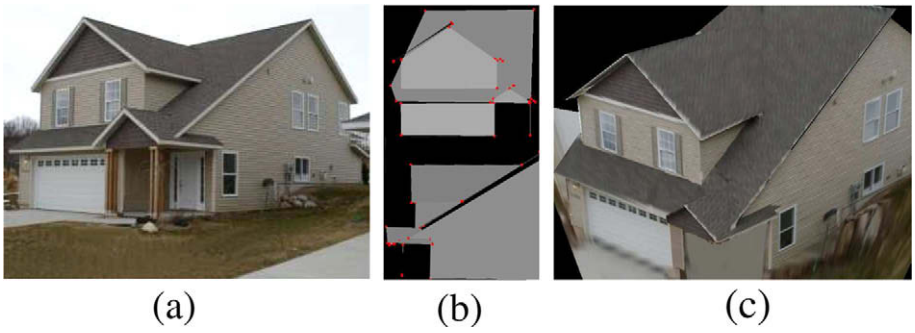

Fig. 10. Reconstruction from a single image: (a) the target image, (b) front and side view of the reconstructed model, and (c) the textured model.

8. Conclusion

In this paper, we have proposed a novel 3D reconstruction method that utilizes both the coplanarities of points and metric constraints (*e.g.*, parallelisms and orthogonalities of planes) simultaneously. Since our method uses both implicit and explicit coplanarities obtained from the laser curves and the planar regions, scenes with complicated and curved surfaces can be densely reconstructed by using a line laser projector. For obtaining a solution, we first obtain a projective reconstruction by solving the linear equations that are derived from the coplanarity constraints. Then, to upgrade the projective solution to the Euclidean space and estimate the camera intrinsic parameters, we solve linear or non-linear equations formulated from the metric constraints. The linear formulation can be solved using linear algebra, and the non-linear formulation can be solved using an optimization method.

In order to verify the reliability and effectiveness of the proposed methods, we conducted a simulation and an actual 3D reconstruction. The results of our experiments confirmed the effectiveness of the proposed method.

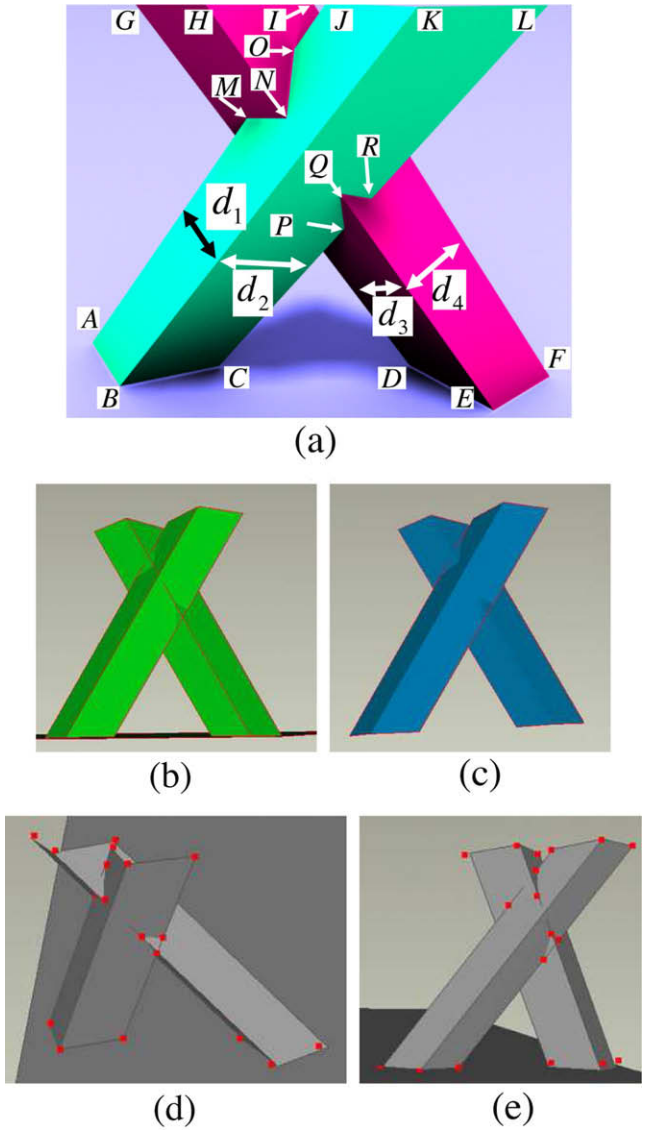

Fig. 11. Reconstruction from the synthetic data: (a) the target scene, (b) the actual 3D model, (c) the reconstructed model rendered from the same view point and direction of (b), and (d) and (e) differences between the actual 3D model and the estimated 3D points.

Acknowledgements

This work was supported in part by SCOPE No. 072103013 (Ministry of Internal Affairs and Communications, Japan) and Grant-in-Aid for Scientific Research No. 19700098 and 21700183 (Ministry of Education, Science, Sports and Culture, Japan).

References

[1] Cyberware, Desktop 3D scanner, <http://www.cyberware.com/>.
[2] L.D. Inc., 3D laser scanners, <http://www.laserdesign.com/>.
[3] F. Blais, Review of 20 years of range sensor development, Journal of Electronic Imaging 13 (1) (2004) 231–243.
[4] M. Ribo, M. Brandner, State of the art on vision-based structured light systems for 3D measurements, Proceedings of International Workshop on Robotics and Sensors Environments.
[5] G.B. Wolfgang Stocher, Automated simultaneous calibration of a multi-view laser stripe profiler, in: ICRA2005, 2005, pp. 4424–4429.
[6] A.M. McIvor, Nonlinear calibration of a laser stripe profiler, Optical Engineering 41 (2002) 205–212.
[7] I.D. Reid, Projective calibration of a laser-stripe range finder, Image and Vision Computing 14 (9) (1996) 659–666.
[8] D. Fofi, J. Salvi, E.M. Mouaddib, Uncalibrated vision based on structured light, in: ICRA, 2001, pp. 3548–3553.
[9] S.Y. Chen, Y.F. Li, Self recalibration of a structured light vision system from a single view, in: ICRA, 2002, pp. 2539–2544.
[10] R. Furukawa, H. Kawasaki, Uncalibrated multiple image stereo system with arbitrarily movable camera and projector for wide range scanning, in: IEEE Conference of 3DIM, 2005, pp. 302–309.
[11] C.W. Chu, S. Hwang, S.K. Jung, Calibration-free approach to 3D reconstruction using light stripe projections on a cube frame, in: Third IEEE Conference of 3DIM, 2001, pp. 13–19.
[12] J.Y. Bouguet, P. Perona, 3D photography on your desk, in: ICCV, 1998, pp. 129–149.
[13] R.B. Fisher, A.P. Ashbrook, C. Robertson, N. Werghi, A low-cost range finder using a visually located, structured light source, in: Second IEEE Conference of 3DIM, 1999, pp. 24–33.
[14] R. Furukawa, H. Kawasaki, Interactive shape acquisition using marker attached laser projector, in: IEEE Conference of 3DIM2003, 2003, pp. 491–498.
[15] R. Furukawa, H. Kawasaki, Self-calibration of multiple laser planes for 3D scene reconstruction, in: 3DPVT, 2006, pp. 200–207.

Please cite this article in press as: R. Furukawa, H. Kawasaki, Laser range scanner based on self-calibration techniques using coplanarities and metric constraints, Comput. Vis. Image Understand. (2009), doi:10.1016/j.cviu.2009.05.006

[16] P. Hebert, A self-referenced hand-held range sensor, in: IEEE Conference of 3DIM2001, 2001, pp. 5–12.
[17] K.H. Strobl, W. Sepp, E. Wahl, T. Bodenmueller, M. Suppa, J.F. Seara,, G. Hirzinger, The dlr multisensory hand-guided device: the laser stripe profiler, in: ICRA2004, 2004, pp. 1927–1932.
[18] Y. Horry, K.-I. Anjyo, K. Arai, Tour into the picture: using a spidery mesh interface to make animation from a single image, in: SIGGRAPH'97, 1997, pp. 225–232.
[19] D. Liebowitz, A. Zisserman, Metric rectification for perspective images of planes, in: CVPR, 1998, p. 482.
[20] P. Sturm, S. Maybank, A method for interactive 3D reconstruction of piecewise planar objects from single images, in: BMVC, 1999, pp. 265–274.
[21] E. Grossmann, D. Ortin, J. Santos-Victor, Algebraic aspects of reconstruction of structured scenes from one or more views, in: BMVC, 2001, pp. 633–642.
[22] E. Grossmann, D. Ortin, J. Santos-Victor, Single and multi-view reconstruction of structured scenes, in: ACCV, 2002, pp. 93–104.
[23] C.-S. Chen, C.-K. Yu, Y.-P. Hung, New calibration-free approach for augmented reality based on parameterized cuboid structure, in: ICCV, vol. 1, 1999, pp. 30–37.
[24] M. Wilczkowiak, E. Boyer, P. Sturm, Camera calibration and 3D reconstruction from single images using parallelepipeds, in: The 8th ICCV, vol. 1, 2001, pp. 142–148.
[25] D. Bondyfalat, B. Mourrain, T. Papadopoulo, An application of automatic theorem proving in computer vision, in: Automated Deduction in Geometry, 1998, pp. 207–231.
[26] M. Wilczkowiak, G. Trombettoni, C. Jermann, P. Sturm, E. Boyer, Scene modeling based on constraint system decomposition techniques, in: ICCV, vol. II, IEEE, 2003, pp. 1004–1010.
[27] D.J. Kriegman, P.N. Belhumeur, What shadows reveal about object structure, Journal of the Optical Society of America 18 (8) (2001) 1804–1813.
[28] H. Kawasaki, R. Furukawa, Dense 3D reconstruction method using coplanarities and metric constraints for line laser scanning, in: IEEE Conference of 3DIM, 2007, pp. 149–158.

Please cite this article in press as: R. Furukawa, H. Kawasaki, Laser range scanner based on self-calibration techniques using coplanarities and metric constraints, Comput. Vis. Image Understand. (2009), doi:10.1016/j.cviu.2009.05.006